Assessment of a photobioreactor-coupled modified Robbins device to compare the adhesion of *Nannochloropsis gaditana* on different materials

O. Zeriouh[1], J.V. Reinoso-Moreno[1], L. López-Rosales[1], M.C. Cerón-García[1,2], A. Sánchez Mirón[1,2], F. García-Camacho[1,2] and E. Molina-Grima[1,2*]

[1]Chemical Engineering Area, University of Almería, 04120 Almería, Spain

[2]Research Center in Agrifood Biotechnology, University of Almería, 04120 Almería, Spain.

Address correspondence to:

E. Molina Grima, Chemical Engineering Area, University of Almería, 04120 Almería, Spain.

E-mail: emolina@ual.es

Phone: 34-950015032

Fax: 34-950015491

Abstract

The prevention of biofouling in the inner walls of closed photobioreactors (PBRs) becomes a critical step in improving the performance of photosynthetic microalgae bioprocesses. Selection of antifouling materials implies approaches at laboratory scale. This work reports the use of a flow cell of the modified Robbins device (MRD) type coupled to a PBR, operated in both batch and continuous modes with the model marine microalgae *Nannochloropsis gaditana* to study the biofouling formation on diverse materials. The fluid-dynamics within the MRD was studied via CFD-aided simulations. At separation distances lower than the cells' diffusion layer thickness, a diffusion-controlled transport of the cells to the material surface was postulated. Results suggested that the flow density of cells in the MRD (J_z), governed by cell concentration gradients, is a significant factor in the adhesion intensity (B) when the PBR is operated in batch mode; not in the continuous mode where the differences observed in B between materials were mainly attributed to the type of material. Polyvinylchloride (PVC) was clearly the best anti-biofouling material compared to polycarbonate, polystyrene, borosilicate glass and stainless steel. The B maximum occurred at the end of the stationary phase in batch culture mode. Continuous culture operation seemed to be preferable since once steady state is achieved, the B value remained low and constant, indicating equilibrium between the number of adhered cells per surface unit and the cell concentration in the culture broth – this was because the adhered cells did not grow on the surface due to phosphate limitation. The PBR-coupled MRD has demonstrated to be well-suited for the screening of antifouling materials under fluid-dynamic conditions relevant in PBRs.

52 **Keywords:** *Nannochloropsis gaditana*; photobioreactor; biofouling; modified Robbins
53 device; computational fluid dynamics

54

55 **Nomenclature**

56 *Acronyms*

CFD	Computational fluid dynamics
GL	Borosilicate Glass
MRD	Modified Robbins device
PBR	Photobioreactors
PC	Polycarbonate
PS	Polystyrene
PVC	Polyvinylchloride
SS	Stainless steel
XDLVO	Eextended Derjaguin-, Landau-, Verwey-, Overbeek model

57

58 *Variables and parameters*

a	Cell radius (m)
A_i	Area that covers each local fluorescence intensity measurement on the test disc coupon (m^2)
A_{TOT}	Total area of the test disc coupon (m^2)
b	Half width of the MRD flow chamber cell (m)
B	Microalgae adhesion intensity (cells m^{-2})
C_b	Nutrient concentration in the bulk culture (mol m^{-3})
C_s	Nutrient concentration on the test coupon surface (mol m^{-3})
D	Dilution rate (day^{-1})

D_H	Hydraulic diameter (m)
D_{II}	Tangential component of the diffusion tensor ($m^2\ s^{-1}$)
d_{max}	Distance to the test coupon surface below which cell-to-surface interactions are significant (m)
D_n	Diffusion coefficient of growth-limiting nutrients ($m^2\ s^{-1}$)
D_T	Normal component of the diffusion tensor ($m^2\ s^{-1}$)
E	Irradiance (μmol photons $m^{-2}\ s^{-1}$)
F_1, F_2, F_3	Universal hydrodynamic functions to correct cell mobility (-)
FI	Chl*a* fluorescence intensity of attached microalgae to coupon surface (au)
F_m	Maximum fluorescence of chlorophyll (au)
F_v	Maximum variable fluorescence of chlorophyll (au)
h	Half depth of the MRD flow chamber cell (m)
H	Separation z-distance normalized by the radius of the cell (-)
J_i	Flow density of cells in the i-direction ($cells\ m^{-2}\ s^{-1}$)
k_B	Boltzmann's constant ($J\ K^{-1}$)
K_m	Mass transfer coefficient for the external liquid film (ms^{-1})
L	Length of the MRD flow channel (m)
n	Cell concentration in the PBR culture ($cells\ m^{-3}$)
N_N	Flow density of dissolved nutrients to the coupon surface ($mol\ m^{-2}\ s^{-1}$)
NO_3^--N_N	Flow density of dissolved nitrate to the coupon surface ($mol\ m^{-2}\ s^{-1}$)
P_e	Peclet number (-)
PO_4^{3-}-N_N	Flow density of dissolved phosphate to the coupon surface ($mol\ m^{-2}\ s^{-1}$)
Q	Volumetric flow rate ($m^3 s^{-1}$)
R_e	Reynolds number (-)
R_H	Hydrodynamic radius of a cell (m)

S_c	Schmidt number (-)
S_h	Sherwood number (-)
T	Temperature (ºC)
U_i	Component of the cell velocity vector in the i-direction (m s^{-1})
V_m	Average flow velocity (m s^{-1})
v_i	Component of the liquid velocity vector in the i-direction (m s^{-1})

Greek symbols

ε	Surface roughness (μm)
δ_D	Thickness of the diffusion boundary layer (m)
δ_H	Thickness of the hydrodynamic boundary layer (m)
μ	Viscosity of the culture broth (Pa·s)
ρ	Density of the culture broth (kg m^{-3})
σ_{xz}	Shear rate on the coupon surface (s^{-1})

Subscripts

x,y,z	Cartesian coordinates components

1. Introduction

The diversity and range of valuable products that can be produced in commercially significant quantities from microalgae is impressive [1, 2]. However, the relatively low production capacity worldwide (about 15,000 tn/year) and the current production costs (> 5 Euro/kg) reduce the possibilities of testing their usefulness in many markets [1, 3]. The economic feasibility of processes based on microalgae biomass requires efficient photobioreactors (PBRs). The prevention of microalgal adhesion to the inner walls of closed PBRs becomes a critical step in improving the performance of photosynthetic microalgae bioprocesses, and consequently, in reducing operating costs [4-6]. When biofouling appears, the possibilities of eliminating it are practically nil, giving rise to a series of detrimental effects that accelerate the culture's collapse. Understanding the factors governing microalgae attachment on PBR surfaces and the impact of hydrodynamics in the vicinity of the PBR wall will enable us to evaluate the probability of adhesion and to predict the adhesion strength, in order to select: (a) materials, and/or coatings, for manufacturing PBRs as a function of the species to be cultured, and (b) the proper fluid dynamics and operational conditions within the PBR [6]. In the PBRs boundary layer, the initial adhesion of the microalga on the surface is governed by a microscopic balance based on the hydrodynamic (lift and drag) and XDLVO (Electrostatic (EL), Van der Walls (LW) and Acid-Base (AB)) forces that act on it [6]. In marine environments, EL forces are negligible due to the high ionic strength of the seawater; in consequence, the LW and AB forces control the adhesion. The surface properties of PBRs, microalga and conditioning film play an important role in initial adhesion. The composition of the conditioning film depends on the composition of the medium (electrolytes, proteins, fatty acids, etc.) and the nature of the surfaces in contact. The adhesion strength microalga-PBRs is the combination of

the adhesion strength microalga-conditioning film and conditioning film-PBRs. One of the most important challenges currently for manufacturers of PBRs is to avoid initial adhesion regardless of the type of microalgae in question and the composition of the medium. In this line, the complicated theoretical analysis of the balance of forces is important to predict the surface properties and the most suitable fluid conditions for the construction and operation of the PBRs.

Parallel-plate flow chamber systems have been reported to be suitable devices for studying not only the deposition of particles [7], but also microbial adhesion to rigid surfaces [8]. The mass transfer in these devices has received considerable attention for a long time due to its great practical significance. Amongst them, the modified Robbins device (MRD) stands out as a widely used laminar flow chamber that houses suspended substrates for analysis of microbial biofilm growth under experimental conditions [9]. MRD can be used in both batch and continuous culture systems [10]. The Robbins device is one of the most commonly used for studying the development of biofilms *in situ* at the real and pilot scale, such as in drinking water distribution systems [11]. Since MRD provides a large number of sample surfaces, when coupled to chemostat bioreactors, the monitoring of biofilm formation and its control over extended periods of time is feasible [12]. Therefore, MRD is presented as an ideal flow cell for studying not only initial adhesion but also the later stages of biofilm formation. Another significant advantage of parallel-plate flow chambers, such as MRD, is that it allows one to study biofilms under flow conditions with controlled hydrodynamics (i.e. shear rate, fluid flow velocity, Reynolds and Péclet numbers, mass transport, etc.) [10, 13]. This is particularly appealing in microalgae cultures because the hydrodynamics and mass transport properties prevailing in the boundary layer adhering to the PBR walls

may be reproduced in an MRD. As far as we know, MRD has never been used in adhesion experiments with microalgae.

A wide variety of results has been reported from numerous studies carried out in parallel-plate flow chambers in order to interpret and predict microbial adhesion to substrata by applying different approaches such as thermodynamics or XDLVO theory. However, this matter has only been comprehensibly reviewed for microorganisms other than microalgae [8, 14] because such studies with microalgae are scarce. In a recent work, it was demonstrated that XDLVO theory may fail to completely predict the adhesion behaviour of the marine microalga *Nannochloropsis gaditana* as it does not take into account other phenomena, such as fluid flow, and therefore the shear forces and mass transport associated with it [6]. Consequently, a detailed study on the mass transport of microalga cells to the PBR wall surface is still lacking; this is because the mass transport and adhesion steps cannot be separated, as demonstrated in particle deposition studies [15].

This study addresses the above-mentioned shortcomings related to microalgal adhesion investigation by means of the following objectives: (i) to monitor the laboratory-scale adhesion dynamics of the marine microalgae *N. gaditana* on diverse materials and under diverse operational conditions similar to those prevailing in outdoor tubular PBRs, in terms of the fluid dynamics and the culture mode; (ii) to relate the fluxes of cells and nutrients to the test material surfaces to the cell adhesion intensity; and (iii) to compare the microalgae cell attachment level on the different materials. For these purposes, a new experimental assembly was developed, where a multi-coupon MRD flow cell was connected in closed circuit to a culture module consisting of a flat-panel PBR. The photobioreactor was operated sequentially in batch and continuous mode. The test materials used in the MRD covered a wide range of physicochemical

properties (i.e. hydrophobic, hydrophilic and metallic): polyvinylchloride (PVC), polycarbonate (PC), polystyrene (PS), borosilicate glass (GL) and stainless steel (SS). These are all commonly used in the manufacture of PBRs. CFD, in combination with basic equations of fluid motion and the continuity general equation, were used for the fluid-dynamic and mass-transfer characterization inside the MRD, as well as for its impact on biofilm development and growth.

2. Materials and Methods

2.1. Microalgae, culture conditions and experimental setup

Monocultures of the microalga *N. gaditana* B-3 were used. The strain was provided by the Marine Culture Collection at the Institute of Marine Sciences of Andalucía (CSIC, Cádiz, Spain). Inoculum was grown in 1-2 L Erlenmeyer flasks under intermittent illumination (12:12 h L:D) at 25 °C; this illumination being provided by 58W fluorescent lamps rendering an average irradiance at the culture flask surface of 100 $\mu E\ m^{-2}\ s^{-1}$. The flasks were agitated by filter-sterilized air sparging injected through a sparger nozzle at an aeration rate of 0.5 $vv^{-1}min^{-1}$. The culture medium was prepared from natural, filter-sterilized (0.22 μm Whatman GF/F 47 mm, Maidstone, The United Kingdom) Mediterranean seawater. The culture medium composition has been reported elsewhere [16].

The experimental setup (see Fig. 1) basically comprised a microalgae culture module (i.e. a PBR) and a cell adhesion module (i.e. a flow cell). The rest were ancillary materials needed for supplying air, CO_2 and culture medium, for controlling pH, conductivity and temperature and for pumping the microalgae culture from the PBR to the adhesion module. A flat-panel photobioreactor was used as the culture system since the existence of significant biofouling in this type of PBR has been confirmed [17]. The

laboratory-scale PBR was made of glass (50 cm wide x 40 cm height x 8.3 cm depth) giving an aspect ratio (area/volume) of 29 m^{-1} with a transparency index of 0.79. The culture volume was fixed at 13.5 L. The PBR was frontally illuminated on both sides with 12 fluorescent lamps (Osram Dulux PRO Mini Twist 23W-840 E27, China) with a 12:12 h L:D illumination cycle. The irradiance was measured using a QSL-100 quantum scalar irradiance sensor. For the purpose of recreating the environmental conditions prevailing in an outdoor PBR that promote biofouling, the irradiance at the centre of the PBR (filled with the culture medium) was fixed at around 1100 μE m^{-2} s^{-1}, the temperature at 26±1 ° and pH at 8.0 ± 0.05. The culture temperature, pH and salinity were controlled as described in a previous work [5].

The adhesion module comprised a MRD flow channel (LPMR-12PMMA, Tyler Research Corp, Edmonton, Canada) with a volume of 12.5mL and a peristaltic pump (Masterflex® L/STM Economy drive) to allow culture broth from the PBR to be pumped into the MRD. The length (L), width (2b) and height (2h) of the flow channel were 173 mm, 9.4 mm and 3 mm, respectively. More details of the MRD can be found in Fig. 2. Briefly, the MRD consisted of two separate halves that were held together by several screws. Connectors at both ends allowed the peristaltic pump to be attached. The lumen was completely within the bottom part of the device with the top half acting as a cover. The upper half of the MRD contained 12 evenly spaced ports which held sample holders with recesses at the ends into which the test disc coupons of the material to be studied were inserted (see Fig. 2). The fluid was allowed to expand stepwise to the flow channel (situated above) at a 40.68º angle, with the first holder situated in the flow channel 0.05 mm from the entry. The MRD was situated 30 cm above the culture module to prevent cell sedimentation within it.

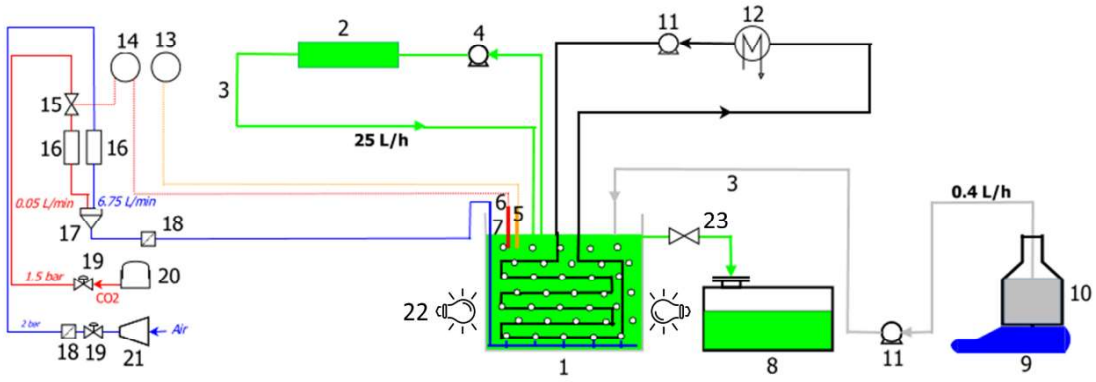

188 **Figure 1.** Flowsheet of the experimental setup. (1) PBR module (Glass, flat-panel
189 photobioreactor). (2) MRD flow cell. (3) Silicone tube. (4) Peristaltic pump. (5)
190 Conductivity cell. (6) pH electrode. (7) Sparger. (8) Harvesting tank. (9) Magnetic
191 stirrer. (10) Culture medium bottle. (11) Centrifugal pump, (12) Water cooler. (13)
192 Conductimeter CM38. (14) Transmitter pH. (15) Solenoid. (16) Flow meter. (17) Mixer.
193 (18) Filter. (19) Adjustable valve. (20) Bottle of CO_2. (21) Compressor. (22) Light
194 panel. (23) Overflow pipe
195

196 Before using the MRD, it was rinsed out with Alcanox® 1% in hot water (40 ºC)
197 and then washed with abundant deionized water. After spending a night immersed in a
198 sodium hypochlorite solution (5%), it was washed again with deionized and sterilized
199 water in a laminar flow cabinet. The silicone tubes that connect the MRD with the PBR
200 were washed with a sodium hypochlorite solution (5%) and rinsed out with deionized
201 water before being autoclaved at 121 ºC for 20 min (Sanyo Labo Autoclave MLS-3780,
202 Sanyo Electric Co., Ltd.). The disc coupon materials mounted in their corresponding
203 holders were also rinsed out by closed-circuit recirculating in hot water (40 ºC)
204 containing 1% Alconox® at a shear rate of 300 s^{-1} (Q= 12.48 L h^{-1}; R_e=300) for one
205 hour. Subsequently, they were washed with deionized and sterilized water under the
206 same conditions at room temperature. Next, a sodium hypochlorite (5%) solution was
207 passed through at the same shear rate by recirculating it in darkness for three hours.
208 Finally, the coupons were washed with abundant deionized and sterilized water. In this
209 work, five rigid materials prepared in the disc coupon form were used (Tyler Research
210 Corp, Edmonton, Canada): PVC, PC, PS, GL and SS. The average roughness (ε) of the

all surfaces tested was determined using a surface profiler (Dektak 150, Veeco Instruments Inc., USA). The ε values for each surface is the average of five measurements at different sites on each surface (scan length = 1mm, resolution = 0.111 microns / sample). The results of ε obtained were the following: ε_{PVC}=0.473±0.022µm, ε_{PC}=0.030±0.003µm, ε_{PS}=0.023±0.003µm, ε_{GL}=0.130±0.010µm and ε_{SS}=0.340±0.040µm. All of them were smooth surfaces (ε <0.6µm).

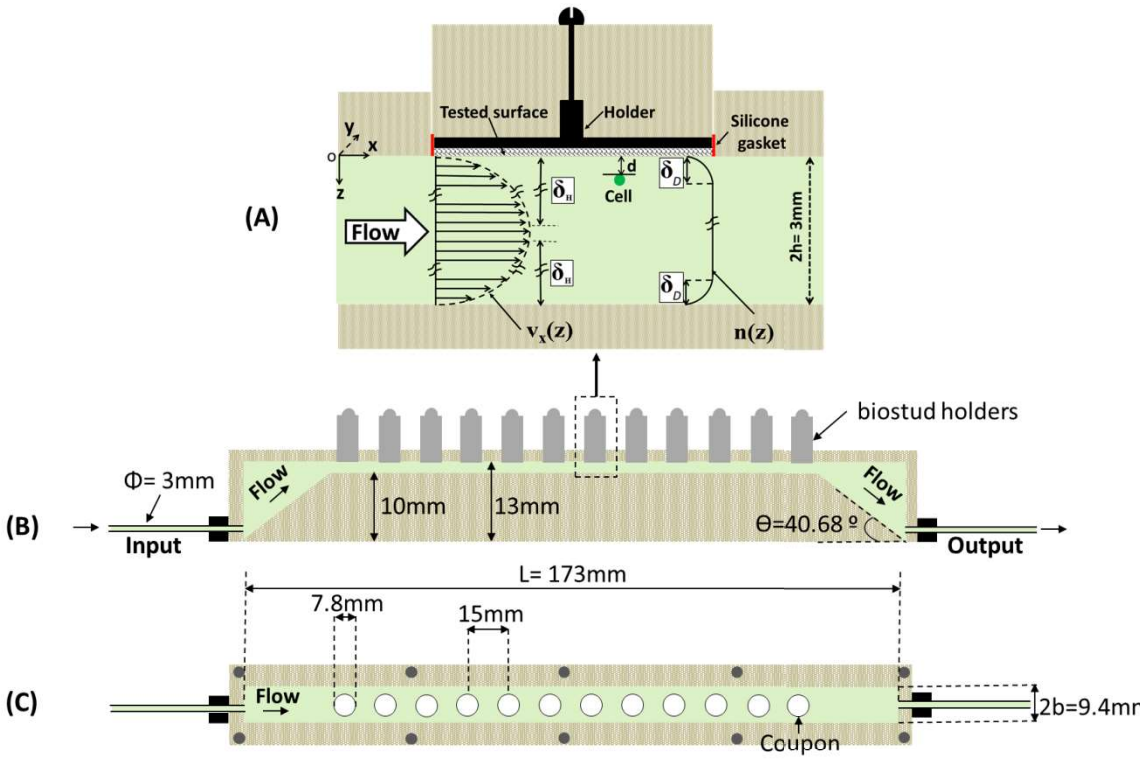

Figure 2. Details of the Modified Robbins Device (MRD). **(A)** Detail of the Biostud holder with the coupon to be tested and its placement in the upper part of the MRD: δ_D and δ_H refer to the thickness of the diffusion and hydrodynamic boundary layer, respectively; v_x(z) and $n(z)$ represent the fluid velocity and cell concentration profiles as a function of the z-component. **(B)** Detailed visualization of a vertical section of the MRD. The biostud holders allow the coupons to be placed in the upper part of the flow cell in such a way that the surfaces of the coupons are practically part of its wall (**C**) Detailed top visualization of a horizontal section of the MRD in the area where the coupons are placed.

2.2. Adhesion experiment

After sterilising the PBR as reported elsewhere [18], it was filled with culture medium. A 9.1L volume of fresh medium was directly inoculated using a 4.5L-sized inoculum that was in the late exponential growth phase. The cell concentration in the freshly-inoculated PBR was approximately 1.8×10^7 cell mL^{-1} (equivalent to a biomass concentration of 0.12 gL^{-1}) and the concentration of the macronutrients phosphates (PO_4^{3-}) and nitrates (NO_3^-) at the beginning of the batch culture was 0.2 mM and 17.65 mM respectively.. The peristaltic pump boosted the PBR culture through a silicone tube to the MRD, and the culture leaving the flow cell was continually recirculated to the PBR. The volumetric flow rate (Q) through the MRD channel was fixed at 25 L h^{-1}, equivalent to an average culture velocity, V_m, through the MRD rectangular channel of 25 cms^{-1}. This ensured that the whole PBR culture volume passed through the adhesion module once every 0.5 hours, equivalent to a culture residence time in the MRD of nearly 1.8s. The recirculation rate was then 48 cycles/day. The experiment started with a culture in batch mode. Once the stationary growth phase was reached, the culture was operated in continuous mode at a dilution rate (D) of 0.33 day^{-1} for a further 9 days. Brieftly, a peristaltic pump daily added 4.5 L of fresh medium to the PBR, while the same amount of culture was continuously harvested through an overflow pipe (See Fig. 1). This mode of operation allows keeping the phosphate concentration low in the PBRs in such a way that it does not affect the growth of the cells in the PBRs and, at the same time, minimize the transfer of nutrients to the cells attached to the surface of the different materials placed in the MRD to limit its growth.

The response variables of the PBR culture measured off-line were the freely-suspended cell concentration in the culture broth, the photosynthetic efficiency of Photosystem II (F_v/F_m), and the phosphate (PO_4^{-3}) and nitrate (NO_3^-) concentrations in

the supernatant. All were determined as described elsewhere [5, 19]. F_V/F_M represents the performance of photochemical processes in PSII and is universally considered to be an indicator of cell stress. The viscosity of the algal suspensions (μ) was measured using a conventional Cannon-Fenske viscometer. The bulk density of the algal suspensions (ρ) was measured using a pycnometer. The viscosity (μ) and density (ρ) at 26 ºC did not change significantly throughout the culture, both being virtually identical to those measured for the culture medium, with values of 0.94×10^{-3} Pa s and 1023 kg m^{-3}, respectively.

2.3. Monitoring microalgal attachment

The microalgal adhesion intensity on the different coupons (B, cells cm^{-2}) was evaluated by measuring the Chlorophyll *a* (*Chla*) fluorescence intensity of the adhered cells (*FI*) on the coupon surface. The relationship between *FI* and *B* was determined as previously described [5]. A linear relationship was observed up to FI<3.1×10^4 (a.u): $FI=3.11\pm0.01\times B$; $r^2=0.982$. Measurements were carried out every two days of culture as follows: Firstly, the peristaltic pump was stopped. Then, the MRD was disconnected from the PBR and connected to a wash module under sterile conditions. The wash module consisted of a 1000 mL vessel with 0.22 µm filtered seawater (this sterilized for 20 min at 121 ºC) and a peristaltic pump (Watson Marlow 101U/R), which boosted the seawater through the MRD at a flow rate of 0.5 Lh^{-1} for 90 min. Under these conditions, the shear rate on the coupon surfaces was 12 s^{-1}, which was still low enough to prevent the cells being removed from the surface. After washing, and under strict sterile conditions in a laminar flow cabinet, the coupons were transferred from the coupon holders to a previously adapted black polystyrene well plate (96-wells, Nunclon®). The well plate was introduced into the multi-well-plate fluorescence reader (SynergyMx,

BioTek® Instruments Inc., USA) and the Chl*a* was excited to 480 nm, measuring the emission at 685 nm. The device scanned the coupon area at 13 different positions. The *B* value was determined averaging these 13 measurements as follows:

$$B = \frac{\sum_{i=1}^{13} Chla_i \cdot 0.3221 \cdot A_i}{A_{TOT}} \quad (1)$$

where A_{TOT} (49 mm^2) is the total coupon area and A_i (3.77 mm^2) is the area covered by each measurement. Once all the coupons were analysed, the adhesion experiment continued by connecting the MRD to the PBR and switching the peristaltic pump on again. The complete operation (i.e. sample washing and adhesion quantification) lasted about 90 min. The protocol herein described allows one to monitor the same coupon through the entire cultivation time, overcoming one of the drawbacks commonly reported for the MRD; namely, having to destruct the coupons for quantitative analysis of the biofilm [10].

2.4. Fluid-dynamic characterization in the MRD flow chamber

For an MRD as described in Fig. 2, the Reynolds number (R_e) of the culture circulating through the flow channel is calculated by the equation

$$R_e = \frac{\rho \cdot V_m \cdot D_H}{\mu} \quad (2)$$

where V_m is the average fluid velocity and D_H is the hydraulic diameter given as

$$D_H = \frac{4 \cdot (2h) \cdot (2b)}{2 \cdot (2h + 2b)} \quad (3)$$

The Navier–Stokes equation in Cartesian coordinates was solved by CFD to simulate fluid velocity and shear stress distributions for the whole MRD flow chamber. Briefly, flow fields were simulated in 3D using the Ansys Fluent® v.16.2 CFD commercial package. Different mesh densities were tested until the solution was

independent of them. The optimal mesh consisted of approximately 2.6×10^6 elements with inflation layers at the wall of the flow channel extending to 500 μm. The first layer height was 0.5 μm to appropriately resolve the boundary layer. The simulations were performed using an HP Z840 Workstation with 2 Intel Xeon® E5-2670v3 processors and 128 GB of RAM.

The axial profile (z direction) of the fluid velocity within the MRD (see Fig. 2A) allowed us to determine the boundary layer to a thickness of δ_H (i.e. the hydrodynamic boundary layer). This corresponds to the distance from the test disc surface at which the fluid velocity is equal to $0.99\times V_m$ and where the mass transport parallel to the surface is convective. Another inner fluid layer of thickness δ_D ($<<<\delta_H$), closer to the coupon surface (i.e. the diffusion boundary layer) was considered (see Fig. 2A), where the mass transport is driven by diffusion and contributes to microalgae transport towards the test disc surface.

Since the y-component of the local fluid velocity (υ_y) is virtually nil in the MRD, the x- and z-components (υ_x and υ_z) are taken into account to characterize the flow field. Note that the cell diameter of *N. gaditana* is about 4 μm (for calculations, the average cell radius, a, was 2 μm) and therefore it is small enough to apply the fine particle deposition and colloidal theories [6]. From the data provided by the CFD simulations, the following simple correlations were found for υ_x and υ_z with the z-distance to the centre of the test disc surface

$$\upsilon_x(z) = 573.84\cdot z \ \ [\mu m\ s^{-1}]\ ;\ r^2=0.999 \tag{4}$$

$$\upsilon_z(z) = -2\cdot10^5\cdot z^3 + 0.0005\cdot z^2 + 0.0044\cdot z \ \ [\mu m\ s^{-1}]\ ;\ r^2=0.999 \tag{5}$$

eqs. (4) and (5) being valid for the dimensionless z-distance H ($=z/a$) between 0 and 7.5 (i.e. $0<z<15$ μm). However, cells subjected to a flow embedded in a fluid, like those circulating inside the MRD, do not follow the streamlines in the vicinity of the coupon

wall and the cell velocity differs from the local fluid velocity at the same point. Fundamentals on uncharged colloidal particle deposition at solid surfaces are described elsewhere [20] and have been used here to take this effect into account. Thus, eqs. (4) and (5) are corrected to calculate the local cell velocity in the vicinity of the test disc surface as follows:

$$U_z(H) = F_1(H) \cdot F_2(H) \cdot \upsilon_z(H) \tag{6}$$

$$U_x(H) = F_3(H) \cdot a \cdot \sigma_{xz} \cdot (1 + H) \tag{7}$$

$$U_y(H) = 0 \tag{8}$$

where σ_{xz} is the shear rate on the coupon surfaces, defined as

$$\sigma_{xz} = \left. \frac{\delta \upsilon_x}{\delta z} \right|_{z=0} \tag{9}$$

and $F_1(H)$ to $F_3(H)$ are correction functions given by

$$F_1(H) = \frac{19 \cdot H^2 + 4 \cdot H}{19 \cdot H^2 + 26 \cdot H + 4} \qquad \frac{d_{max}}{a} < H < 2 \tag{10}$$

$$F_2(H) = 1 + \frac{1.79}{(0.828 + H)^{1.167}} \qquad \frac{d_{max}}{a} < H < 2 \tag{11}$$

$$F_3(H) = \frac{1}{0.754 - 0.256 \cdot \ln(H)} \qquad \frac{d_{max}}{a} < H < 0.137 \tag{12}$$

$$F_3(H) = 1 - \frac{0.304}{(1 + H)^3} \qquad 0.137 \le H < 2 \tag{13}$$

where d_{max} is the z-distance to the coupon surface below which cell-to-surface interactions are significant and should be considered. A conservative value of 100nm was used here, in line with previous studies [21, 22].

2.5. Transport of cells and nutrients to the disc coupon surfaces

For the Q value (=25 L h^{-1}) fixed in the MRD, the culture flow is laminar (R_e=1215) and steady in most parts of the channel (see Section 3.2). Assuming that the

337 interactions between the cells can be disregarded, the general continuity equation in the
338 steady state (i.e. $\partial n/\partial t = 0$) for a incompressible fluid (i.e. culture broth) circulating
339 through the MRD can be written in the form [7]

$$\frac{\partial J_x}{\partial x} + \frac{\partial J_y}{\partial y} + \frac{\partial J_z}{\partial z} = 0 \tag{14}$$

340 where J_x, J_y and J_z are the respective components of the microalgae cells' flux density
341 vector given as

$$J_x = -D_{II} \cdot \frac{\partial n}{\partial x} + U_x \cdot n \tag{15}$$

$$J_y = -D_{II} \cdot \frac{\partial n}{\partial y} + U_y \cdot n \tag{16}$$

$$J_z = -D_T \cdot \frac{\partial n}{\partial z} + U_z \cdot n \tag{17}$$

342 where D_{ll} and D_T are the tangential and normal components of the diffusion tensor,
343 respectively; U_x, U_y and U_z are the microalgae cell velocity vector components deriving
344 from all the forces acting on the cell and n is the freely-suspended cell concentration in
345 the culture broth.

346 The following assumptions have been adopted in order to simplify the
347 application of Eq. (14) to the MRD: (i) as v_y is virtually nil, $U_y=0$; (ii) there is only a
348 cell gradient in the z-direction (i.e. $\partial n/\partial x=0$, $\partial n/\partial y=0$, $\partial n/\partial z\neq 0$); (iii) the velocity of
349 microalgae cells in the x-direction, U_x, is constant; (iv) cell-to-surface interactions are
350 not significant when cells are at a distance from the wall above d_{max}. Thus, Eq. (14) is
351 simplified to

$$D_T \cdot \frac{\partial^2 n}{\partial z^2} + U_z \cdot \frac{\partial n}{\partial z} + \frac{\partial U_z}{\partial z} \cdot n = 0 \tag{18}$$

352 Resolving Eq. (18) allows us to determine the microalgae cell concentration gradient in
353 the z-direction, $n(z)$ (i.e. the normal direction to the disc surfaces), and therefore

354 estimate the diffusion boundary sub-layer thickness, δ_D. A D_T value of 1.2×10^{-13} m^2s^{-1}
355 was estimated with Einstein's equation [8],

$$D_T = \frac{k_B \cdot T}{6 \cdot \pi \cdot \mu \cdot R_H} \tag{19}$$

356 where R_H is the hydrodynamic cell radius (an average cell radius of 2μm was used) and
357 k_B is the Boltzmann constant. Eq. (17) has been used to estimate the flux density of the
358 microalgae cells, J_z (cell cm^{-2} s^{-1}), approaching the test disc surfaces.

359 On the other hand, there is also a flux density of nutrients (N_N) from the culture
360 broth circulating through the MRD to the test disc surfaces. This flux is responsible for
361 depositing nutrients onto the test disc surfaces to create a conditioning film prior to
362 biofouling and it also remains once the microalgae has formed a biofilm on the surface.
363 Since N_N mainly occurs as a result of convective mass transfer and diffusion, it can be
364 expressed as reported elsewhere [23],

$$N_N = K_m \cdot (C_b - C_s) \approx K_m \cdot C_b \tag{20}$$

365 where K_m is the external liquid mass transfer coefficient, while C_b and C_s are the nitrate
366 and phosphate concentrations in the culture broth and on the coupon surface,
367 respectively. Here, nitrates and phosphates were considered to be the potentially
368 growth-limiting nutrients. In general, $C_b >> C_s$ and hence, the driving force in Eq. (20)
369 is reduced to C_b. The rate constant K_m is related to the Sherwood number (S_h) by:

$$K_m = \frac{S_h \cdot D_n}{D_H} \tag{21}$$

370 where D_n is the aqueous diffusion coefficient of the growth-limiting nutrient. Under
371 laminar flow conditions ($500<R_e<2000$), the following empirical equation to calculate
372 S_h in the MRD flow channel is recommended [24];

$$S_h = 2 \cdot P_e^{0.5} \cdot \left(\frac{D_H}{L} \right)^{0.5} \cdot \left(1 + 0.0021 \cdot R_e\right) \quad (22)$$

where P_e is the Péclet number, which denotes the ratio between the convective and diffusional mass transport in the MRD, and is calculated as follows:

$$P_e = R_e \cdot S_c \quad (23)$$

where S_c is the Schmidt number given by

$$S_c = \frac{\mu}{D_n \cdot \rho} \quad (24)$$

Microalgae attached to conditioning films may be more active than free-living cells as has been observed for cells other than microalgae [25]; this is because the diffusion distance is shorter and, consequently, the mass transfer is faster. In this case, Eq. (20) may underestimate N_N in the end.

Regarding macronutrients, the value of D_n for phosphate was assumed to be similar to that for nitrate in water (1.4×10^{-9} m^2 s^{-1}), as reported elsewhere [26]; four orders of magnitude higher than the diffusion coefficient (D_T) computed for *N. gaditana* cells. The estimated values of S_h and P_e (1027 and 7.9×10^5, respectively) for the macronutrients indicated that nutrient transport within the MRD was dominated by convection and the culture flow had plug-flow behaviour. The estimated K_m value was 3.15×10^{-4} m s^{-1}. Replacing D_n with D_T in the Schmidt number (Eq. (24)), the S_c and P_e values for *N. gaditana* cells were 7.8×10^6 and 9.4×10^9, respectively. This means that the convective transport of cells within the MRD was nearly nine orders of magnitude greater than that for diffusive transport.

2.6. Statistical analyses

Statgraphics centurion XVII version 17.2.04 statistical software (2014 Statpoint Technologies, Inc. USA) was used for: (i) A significant difference analysis with a One-way ANOVA test (ii) A significant difference analysis with a Multi-way ANOVA test.

3. Results and discussion

3.1. Fluid dynamics within the MRD

Fig. 3 displays the results from CFD modelling in terms of the culture velocity, the shear rate and the streamlines within the MRD including the vicinity of the test disc surfaces. Although the culture flow was laminar (R_e=1225), flow disturbances can be observed in Fig. 3A, which are generated by the inlet and outlet connexions of the MRD and by the effects of the MRD lateral walls (Fig. 3A). This represents a deviation from the ideal full flow developed in most parts of the rectangular channel, as is commonly observed in parallel-plate flow channels [27]. As a result, non-unidirectional velocity profiles arose at different sites in the rectangular flow channel, where the biostud holders are located (see Fig. 3B).

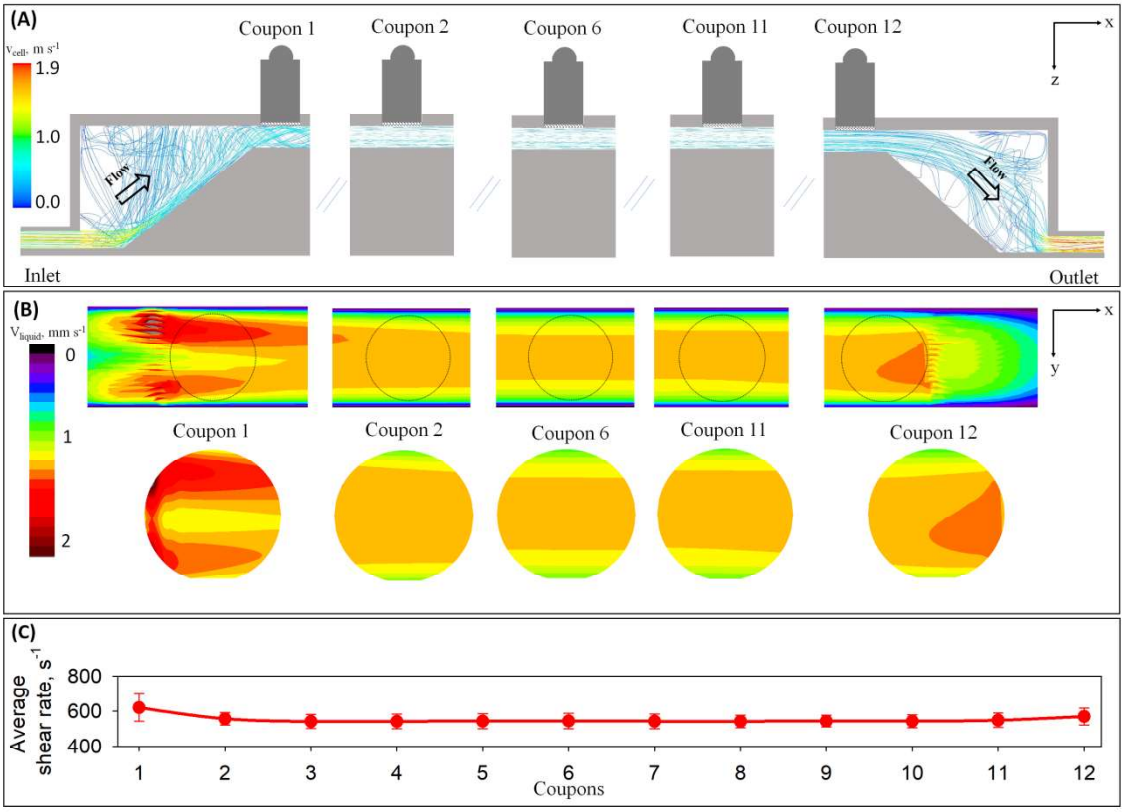

Figure 3. Fluid-dynamic description of the modified Robbins device (MRD) from CFD simulations for the culture flow rate tested (Q= 25Lh^{-1}, Re=1215). **(A)** Detailed visualization of streamlines for a vertical section of the MRD. Three different zones are shown: the entrance, sampling and exit zones. The entry and exit zones show a turbulence flow in the streamlines because of abrupt changes in the hydraulic diameter and flow direction. At the entrance, the streamlines are directed towards the surface of the first coupon, while at the exit, they move away from the twelfth coupon. In the sampling zone (coupons 2-11), the streamlines were stable and practically parallel. **(B)** Velocity contour plots at 2 µm (equivalent to the cellular radius) of the surface of the coupons. The velocity profile for coupon 1 and 12 (entry and exit zones) and coupons 2, 6 and 11 (the sampling zone) are drawn. The circles drawn with dotted lines indicate the position of the coupons and the zoom of each coupon can be seen just below. Coupons 1 and 12 show heterogeneous velocity profiles and an average velocity greater than that of coupons 2-11, which presented a homogeneous velocity pattern, stable and similar. **(C)** Average shear rate on each coupon simulated by CFD. The vertical bars are standard deviation. The average shear rate values on coupons 1 and 12 were higher compared to the intermediate coupons (2-11), which presented similar average shear rate values.

Apparently, the MRD design was originally conceived to eliminate undesirable entry effects in the flow developing in the area where the coupons are located. For this reason, right before and after the rectangular flow channel, the MRD has a triangular-shaped chamber (see Fig. 2 and 3). In these chambers, the streamlines are intentionally

unordered to stabilize the flow right before and after the entrance and exit to the rectangular channel, respectively. However, at the entrance of the rectangular channel, the streamlines are not yet completely parallel and are directed towards the surface of the first coupon, whilst at the exit, they move away from the twelfth coupon. In contrast, the streamlines are stable and practically parallel in the zone occuped by coupons 2 to 11. Consequently, the fluid velocity field at an *z*-plane located 2 μm from the surface of the disc coupons (Fig. 3B) was significantly different between both the first and last coupons than for the rest of them (2-11). Similarly, the average shear rate (σ_{xz}) remained practically constant (≈545±5 s^{-1}) from coupon 2 to 11, increasing in the two peripheral coupons (Fig. 3C). Consequently, only holders 2 to 11 were used to allocate coupons since this section of the rectangular channel provides the flow stabilization length required to allow direct comparison of the biofouling observed in the different coupons [28].

3.2. Culture experiment in the flat-panel photobioreactor

Fig. 4A shows the dynamics of the culture in the PBR operated sequentially in batch and continuous modes. The culture was inoculated at 1.8×10^7 cell mL^{-1} (equivalent to a biomass concentration of 0.12 gL^{-1}) and operated in batch mode over the first 11 days. After a lag phase which lasted for 2 days, the culture entered the exponential growth phase and the maximum growth rate (μ_{max}) is 0.51 $days^{-1}$. On day 2, the culture module was connected to the MRD. On day 6, due to nutrient depletion, the culture started the linear growth phase until it reached the stationary growth phase, in which a cell concentration of 3.15×10^8 cell mL^{-1} was achieved. From day 11 onwards, the culture module was operated in continuous operational mode at a dilution rate of D=0.33 day^{-1} (i.e. one third of the volume of the culture within the PBR was harvested daily; namely,

4.5 L over 10 hours at a flow rate of 0.45 L h^{-1}; simultaneously, this was replaced by the same flow rate of culture medium). A steady-state cell concentration of about 2.4×10^8 cell mL^{-1} (equivalent to a mass concentration of 1.1 gL^{-1}) was reached. Conversely, the phosphate concentration in the PBR dropped markedly to almost zero on the 6th day while the nitrate concentration decreased from an initial 17 mM to 7 mM and remained almost constant for the rest of the experiment. During the continuous operation mode, the phosphate concentration was also low, and the nitrate remained constant at 7.5±1.2 mM. The photosynthetic efficiency of Photosystem II (F_v/F_m) varied in the 0.64-0.70 range throughout the experiment, demonstrating significant culture robustness throughout the experimental period. These values of F_v/F_m, are characteristic of a healthy culture of *N.gaditana* as reported for a similar PBR [5]. F_v/F_m is considered to be the most vulnerable component of the photosynthetic machinery and therefore an excellent sensor of the cell response to environmental and operation conditions. In this sense, the coupling of the MRD to the PBR did not seem to affect the efficiency of the PBR culture.

3.3. Transport of cells and nutrients to the test surfaces.

It has been documented in studies carried out on a number of microalgae species that the adhesion density increases with the cell concentration of the suspension [29]. This suggests that the flow density of cells (J_z) in the MRD, governed by cell concentration gradients, is a significant factor in the adhesion rate. On the other hand, the microalgae cells attached to the material surfaces need nutrients to grow or simply stay viable. Therefore, the flow density of nutrients reaching the test coupon surface (N_N) in the MRD also plays an important role in the development of microalgal biofouling. For this reason, flow densities throughout the PBR culture for the dissolved

nitrate (NO_3^--N_N) and phosphate (PO_4^{3-}-N_N), as well as for the cells (J_Z), from all the culture broth circulating through the MRD to the test disc surfaces were estimated.

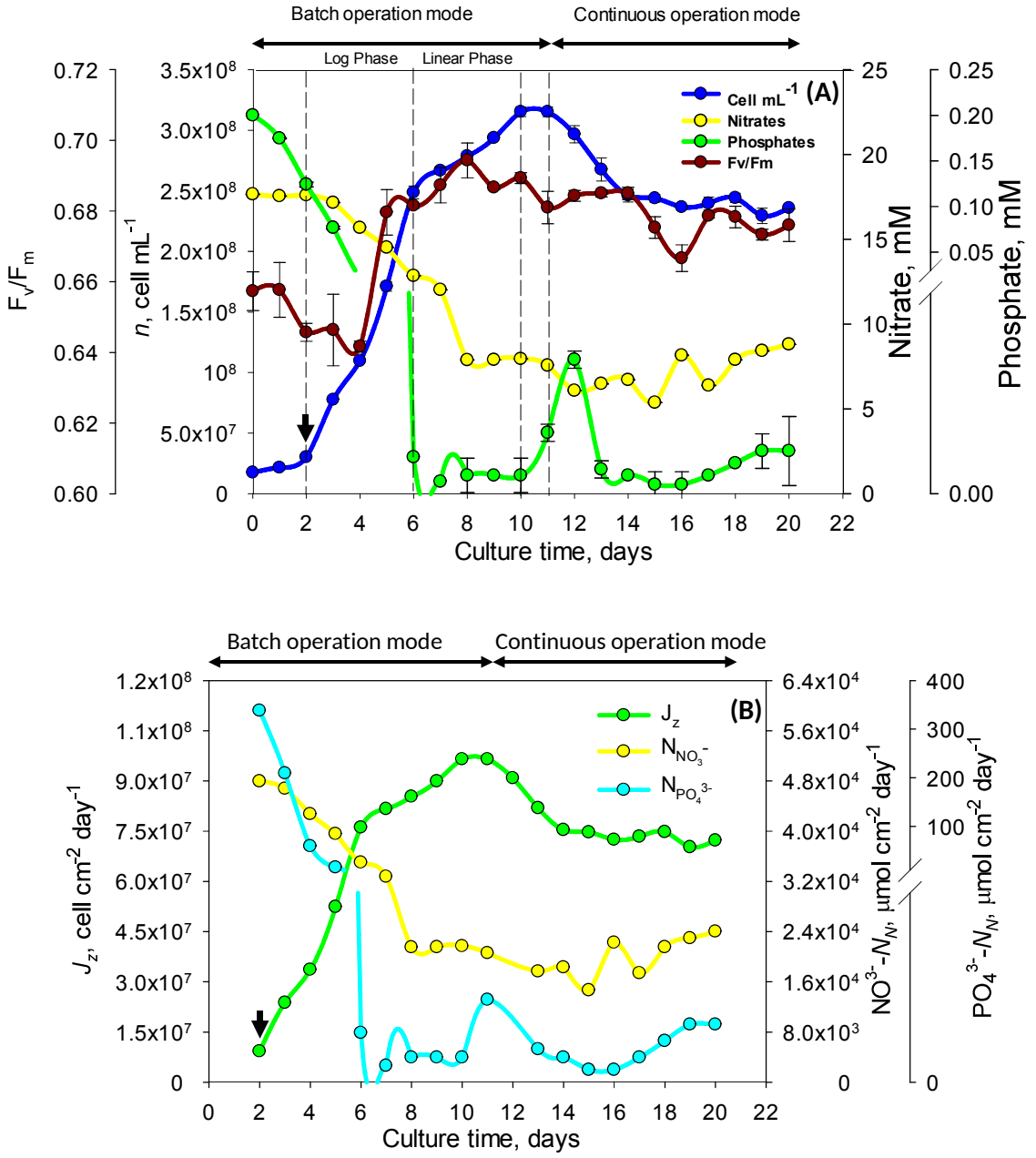

Figure 4. **(A)** Dynamics of the culture in the glass flat-panel laboratory PBR (culture module) operated sequentially in batch and continuous modes. Evolution of the freely-suspended cell concentration of *N. gaditana* (n), F_v/F_m, nitrate ([NO_3^-]) and phosphate ([PO_4^{3-}]) concentrations. Data points are averaged values, and vertical bars are standard deviation for triplicate samples. (**B**) Evolution of the flow density of nitrates (N_{NO3^-}) and phosphates ($N_{PO4^{3-}}$) calculated with Eq. (20), and of microalgae cells (J_z) with Eq. (17) at a distance of d_{max} (=0.1µm) of the surface of disc coupons located in the MRD. The arrow indicates the day on which the flow cell (MRD) was connected in closed loop to the PBR.

According to Section 2.2 above, J_Z is relevant in the vicinity of the test disc surfaces, i.e. $z<d_{max}$. In this zone, the estimated values for the thickness of the diffusion layer (δ_D) and the hydrodynamic boundary layer (δ_H) were 5-6μm and 1022μm, respectively. As expected, δ_D is significantly lower than δ_H. In Fig. 2A, the cell concentration profile, $n(z)$, determined from Eq. (18) is represented. It can be observed that $n(z)$ is flat for $z>\delta_D$, which is consistent with results reported for colloidal particles and microorganisms other than microalgae cells [7, 8, 15]. From separation distances $z<\delta_D$, a gradient of n in the z-direction is established (see Fig. 2A), typical of a transport of cells dominated by diffusion.

Fig. 4B illustrates the dynamics of NO_3^--N_N, PO_4^{3-}-N_N and J_Z in the MRD during the culture period. The J_Z values displayed correspond to those computed at a separation distance $z=d_{max}$. As expected from Eq. (20), the evolution of NO_3^--N_N and of PO_4^{3-}-N_N resemble the variations in nitrate and phosphate concentrations in the PBR culture. The NO_3^--N_N value dropped from 4.8×10^4 μmol cm^{-2} day^{-1} (day 2) to 2.1×10^4 μmol cm^{-2} day^{-1} (day 8) and later stayed constant in all the experiment at $(1.99\pm0.3)\times10^4$ μmol cm^{-2} day^{-1}. With respect to phosphates,the PO_4^{3-}-N_N significantly decreased from 338 μmol cm^{-2} day^{-1} (day 2) to 0.25 μmol cm^{-2} day^{-1} (day 10). When the PBR was operated in continuous mode, the phosphates fed with the culture medium were taken up by the microalgae cells in suspension and the PO_4^{3-}-N_N value was approximately 0.50 μmol cm^{-2} day^{-1}. Similarly, the tendency of J_Z matched the change in cell concentration, when the PBR was operated in batch mode (days 2-11); J_Z varied from 9.2×10^6 cells cm^{-2} day^{-1} (day 2) up to 9.6×10^7 cells cm^{-2} day^{-1} (days 10-11). During the steady state of continuous operation mode the J_z value was established at 7.3×10^7 cells cm^{-2} day^{-1}.

As will be discussed below, J_Z cannot justify cell adhesion *per se* on any surface because the material type may affect the distribution of interaction forces between

surface and cells. On the other hand, cell-to-surface interactions occur at a separation distance below d_{max} ; which, although fixed at 100nm, is really material-dependent (see Section 2.4). Only the cells reaching separation distances $z \leq d_{max}$ are more likely to adhere to the material surface, and only a fraction of them do so. The microalga *N. gaditana* has a hydrophilic surface [5]. On the hydrophobic surfaces (PVC, PS, SS and PC, in decreasing order of hydrophobicity) the hydrophobic attractions are dominant and adhesion usually occurs at primary minimums, where adhesion is irreversible, and the adhesion strength increases as surface hydrophobicity increases [22]. However, on the hydrophilic surfaces (GL), although there are repulsions of hydration due to the hydration layer on the surface, the Van der Walls forces make the adhesion occurs in a primary energetic minimum [22] and the reversibility of the adhesion will depend on the magnitude of this.

3.4 Biofouling development in different materials

Fig. 5 presents the temporal variation in the number of adhered cells per surface unit (B) on the different materials located in the MRD and exposed continuously to culture broth from the photobioreactor. The dynamics of B closely resembled that of J_Z represented in Fig. 4B; that is, B generally increased during batch mode operation until reaching a maximum value in the stationary phase and the beginning of the continuous culture mode. Subsequently, B dropped abruptly, remaining virtually constant from day 12. The PVC coupon was an exception because its B values were the lowest and did not vary significantly from the second day of exposure ($p<0.05$), as appreciated in Fig. 5. Interestingly, the maximum B values observed depended not only on J_Z (as may be reasonably expected), but also on the type of material. More specifically, in batch operation mode, 68% of the variation in B was explained by J_z and 24% by the type of

material (multi-factor ANOVA; F_{Jz}=8.66, $p<0.05$; $F_{Materials}$=3.01, $p<0.05$). The highest average value of *B* was observed for the *PS* material (nearly $2.1x10^5$ cells cm^{-2}) on day 10 of exposure, followed by the *GL*, *PC*, *SS* and *PVC,* with 250%, 500%, 490% and 1650% less, respectively, compared to *PS* material. When investigating the effect of J_z on the adhesion density *B* separately for each material, J_z has significant influence on the values of *B* and their contribution varies from one material to another (F_{SS}=194; F_{PC}=98; F_{PS}=29; F_{GL}=11; $p_{all\text{-}materials}<0.05$). The significant influence of J_z on the adhesion indicates a clear relation between the transport of the cells to the surface and the probability of adhesion, especially, in the first six days of exposure, where significant difference of *B* between one material and another was not observed. Excluding PVC, which as said before is the best antibiofouling surface tested, with the lowest B values and did not change significantly, the materials with less adhesion density, i.e. SS and PC, were more influenced by J_z than the materials (PS and GL) that had higher adhesion levels. The average of the area occupied by the adherent cells (number of adhered cells multiplied by the area occupied by each cell) respecting the total surface area of each coupon (PS, GL, PC and SS) at 10 days of exposure was 42%, 17%, 9% and 8%, respectively. The degree of J_z induction is in accordance with the area occupied by the adhered cells. On the one hand, more adhered cells implies more free surface area between the adhered cells blocked for adhesion of new cells. On the other hand, the cell-cell interactions are less favourable due to the hydrophilic nature of the *N. gaditana*. Other factors could justify the level of the number of cells adhered on the surfaces of GL and PS such as the growth of adhered cells. The different levels of adhesion observed on the different materials at 8-10 days of exposure indicates that the surface properties of the material play an important role in cell-surface interactions. In decreasing order, the greatest interaction forces are observed on the PS, GL, PC, SS and

PVC. Unlike the MRD, the cell-to-material contact under static culture broth conditions is hardly representative of PBR systems, where the fluid dynamics are a crucial factor in cell adhesion. Nevertheless, it was also reported that the PS material was far more prone to undergo cell attachment compared to *PC*, *SS* and *PVC,* when materials were submerged in Petri dishes containing a static suspension of the freshwater microalgae *Chlorella vulgaris* [30]. This observation is consistent since the surfaces of *C. vulgaris* and *N. gaditana* are hydrophilic, and the surface free energy and cell size of both species are similar [4, 5]. Therefore, similar cell surface properties should imply similar adhesion responses.

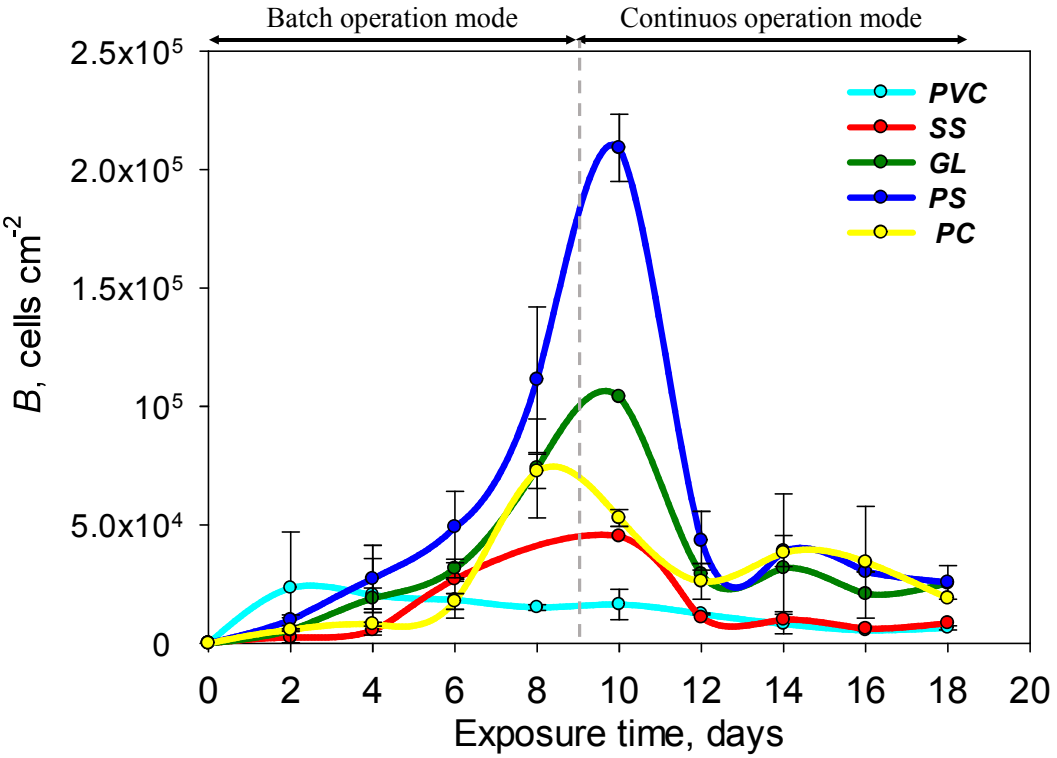

Figure 5. Evolution of the adhesion intensity (*B*) of *N. gaditana* for the different materials tested as a function of the culture operational mode. The monitoring of the adhesion started on the second day, once the MRD and PBR were connected. Data points are averages, and vertical bars are standard deviation (SD) for duplicate samples.

With respect to the effect of continuous culture mode on biofouling formation, values for *B* were markedly lower than the maximum ones measured during the batch culture (see Fig. 5). Since quasi-steady state values for J_Z and *B* were simultaneously attained at the same culture time on day 13, a nearly constant *B* to J_Z ratio was observed during this period. As a result, the differences observed in the adhesion intensity (i.e. *B*) between materials were attributed to the type of material by nearly 90% ($F_{Materials}$=17.04; $p<0.05$) and not to J_Z (F_{Jz}=2.40; $p>0.05$). As in batch mode, *PVC* was clearly the best anti-biofouling material. However, in contrast to batch mode, continuous culture distributed the test materials into two groups that were essentially statistically different in terms of *B*: (i) *PVC* and *SS* with an adhesion intensity of around $1x10^3$ cells cm^{-2}; and (ii) *PS*, *GL* and *PC*, which were approximately 350% higher. Apparently, constant values of *B* are consistent with a probable quasi-steady state balance between several processes that have different time scales: cell attachment, the growth of the attached cells and their detachment – all occur simultaneously in series-parallel with complex dynamics, as previously reported [26]. This equilibrium was unbalanced during the batch culture as deduced from the variable and non-proportional *B* to J_Z ratio. During this period, processes of adhesion and attached cell growth seem to be clearly dominant. In contrast, the first two days corresponding to continuous mode (see Fig. 5), just before reaching quasi-steady state, were characterized by a strong cell detachment rate – an observation compatible with aging cells from the batch culture that are weakly adhered to the test material surfaces and feebly embedded in the biofouling layer. This pattern was also described for non-microalgal cells [8, 26].

Interestingly, the intensity of the attached cell growth seemed to be regulated mainly by the culture mode. Electrolytes such as phosphate and nitrate had two ways to be accessible to the cells: (i) accumulating in the hydration layer of a few nanometres

surrounding the *N. gaditana* cells due to its hydrophilic nature [6, 21, 31]; or (ii) adsorbed on the test surfaces [32]. The cells directly attached to test surfaces have two sources of nutrients. However, the contribution of the second is likely to be more irrelevant than the first because *N. gaditana* has high sphericity (>0.8) and, therefore, the cell surface in contact with the coupon surface is small compared to the free cell surface exposed to the hydration layer. This is supported by the dynamics of NO_3^--N_N and PO_4^{3-}-N_N (Fig. 4B) and *B* (Fig. 5). The high values of NO_3^--N_N (4.8×10^4 μmol cm^{-2} day^{-1} , day 2) and PO_4^{3-}-N_N (338 μmol cm^{-2} day^{-1}, day2) at the beginning of the batch culture period caused an excess of nutrient availability compared to the continuous culture mode, where nutrients were fed into the PBR at a rate that allowed their concentrations to diminish notably in the broth, particularly phosphate (NO_3^--N_N = $(1.99\pm0.3)\times10^4$ μmol cm^{-2} day^{-1} and PO_4^{3-}-N_N= 0.50 μmol cm^{-2} day^{-1}). As a result, microalgae adhering to the test disc surfaces or embedded into the biofilm continuously experienced reduced nutrient flux densities that limited their growth.

From a practical point of view, the results presented here are interesting in addressing PBR design and operation. The MRD is revealed as a valuable tool in screening non-supporting surfaces for microalgal biofilm because it can run for very long periods without intervention and the test material coupons can be extracted and inspected. The MRD is also suitable for flow experiments aimed at evaluating the fluid-dynamic conditions relevant in PBRs. Presumably, continuous culture operation is preferable in PBRs since it may reduce the growth of adhered cells and hence delay biofouling formation. Alternatively, the batch culture phase just after inoculating the PBR may be substituted by a fed-batch mode since this would guarantee low nutrient concentrations in the broth and, consequently, diminished the probability of biofouling.

4. Conclusions

The most relevant results of this work are that: (1) the fluid-dynamic conditions in the MRD were similar for all the coupons tested; (2) in discontinuous operation mode (except for PVC), the evolution of cell adhesion intensity followed a pattern similar to the concentration of freely-suspended cells in the PBR or the flux density of the cells, but were not proportional – meaning that other factors affect the net attachment of cells, such as the growth of biofilm-embedded cells and detachment; (3) except for PVC, which presented the maximum adhesion peak after 2 days of exposure, the maximum adhesion values were observed at the end of the stationary growth phase when the culture was operated in batch mode and growth was nutrient limited; (4) the cells adhered per surface unit remained constant for all surface materials when the PBR was operated in continuous mode; this was because of phosphate limitation; (5) implementing limitations of an essential growth nutrient, such as phosphates, in the PBRs limits this nutrient's transfer to the surface; therefore the formation of macrofouling in the photobioreactors is kept low, which slows the growth of adhered cells on the surface (6) PVC and SS present lower average adherent cells compared to the rest of the materials, PC, GL and PS. Ongoing work is addressing the relationship between the number of adhered cells per unit area and the surface properties of the different tested disc surfaces.

Acknowledgements

This research was funded by the Spanish Ministry of Economy and Competitiveness Projects CTQ2013-46552-R, CTQ2014-55888-C3-02 and the European Regional Development Fund Program. O. Zeriouh wishes to thank the Ministry of Economy and Competitiveness for the grant awarded to carry out the doctoral thesis.

Author contributions

All authors have made substantial contributions to the conception and design of the study, acquisition of data, analysis and interpretation of data, drafting the article or revising it critically for important intellectual content final approval of the version. The following authors take responsibility for the integrity of the work as a whole, from inception to finished article: O. Zeriouh (oz148@ual.es), F. García-Camacho (fgarcia@ual.es) and E. Molina-Grima (emolina@ual.es).

Conflict of interest

The authors declare no conflict of interest.

Statement of informed consent, human/animal rights

No conflicts, informed consent, human or animal rights applicable

Declaration of authors' agreement

All authors agree on the authorship and submission of the manuscript to Algal Research for peer review

References

[1] F.G. Acién, J.M. Fernández, E. Molina-Grima, Economics of microalgae biomass production, in: A. Pandey, D.J. Lee, Y. Chisti, C.R. Soccol (Eds.) Biofuels from Algae, Elsevier, San Diego, 2014, pp. 313-325. DOI: 10.1016/B978-0-444-59558-4.00014-0

[2] O. Pulz, W. Gross, Valuable products from biotechnology of microalgae, Appl. Microbiol. Biotechnol., 65 (2004) 635-648. DOI: 10.1007/s00253-004-1647-x

[3] Y. Chisti, Biodiesel from microalgae beats bioethanol, Trends Biotechnol., 26 (2008) 126-131. DOI: 10.1016/j.tibtech.2007.12.002

[4] M. Sirmerova, G. Prochazkova, L. Siristova, Z. Kolska, T. Branyik, Adhesion of *Chlorella vulgaris* to solid surfaces, as mediated by physicochemical interactions, J. Appl. Phycol., 25 (2013) 1687-1695. DOI: 10.1007/s10811-013-0015-6

[5] O. Zeriouh, J.V. Reinoso-Moreno, L. López-Rosales, B. Sierra-Martín, M.C. Cerón-García, A. Sánchez-Mirón, A. Fernández-Barbero, F. García-Camacho, E. Molina-Grima, A methodological study of adhesion dynamics in a batch culture of the marine microalga *Nannochloropsis gaditana*, Algal Res., 23 (2017) 240-254. DOI: 10.1016/j.algal.2017.02.008

[6] O. Zeriouh, J.V. Reinoso-Moreno, L. López-Rosales, M.C. Cerón-García, A. Sánchez-Mirón, F. García-Camacho, E. Molina-Grima, Biofouling in photobioreactors for marine microalgae, Crit. Rev. Biotechnol., 37 (2017) 1006-1023. DOI: 10.1080/07388551.2017.1299681

[7] Z. Adamczyk, T.G. Van De Ven, Deposition of particles under external forces in laminar flow through parallel-plate and cylindrical channels, J. Colloid Interface Sci., 80 (1981) 340-356. DOI: 10.1016/0021-9797(81)90193-4

[8] R. Bos, H.C. Van der Mei, H.J. Busscher, Physico-chemistry of initial microbial adhesive interactions–its mechanisms and methods for study, FEMS Microbiol. Rev., 23 (1999) 179-230. DOI: 10.1111/j.1574-6976.1999.tb00396.x

[9] J.W. Nickel, J.C. Costerton, T.I. Ladd, Suitable methods for the comparative study of free-living and surface-associated bacterial populations, in: J.S. Poindexter, E.R.

Leadbetter (Eds.) Methods and special applications in bacterial ecology, Plenum, N.Y., 1986, pp. 49-84.

[10] L. Hall-Stoodley, J.C. Rayner, P. Stoodley, H.M. Lappin-Scott, Establishment of Experimental Biofilms Using the Modified Robbins Device and Flow Cells, in: C. Edwards (Ed.) Environmental Monitoring of Bacteria, Humana Press, Totowa, NJ, 1999, pp. 307-319. DOI: 10.1385/0-89603-566-2:307

[11] I. Gomes, M. Simões, L.C. Simões, An overview on the reactors to study drinking water biofilms, Water Res., 62 (2014) 63-87. DOI: 10.1016/j.watres.2014.05.039

[12] J. Jass, J.W. Costerton, H.M. Lappin-Scott, Assessment of a chemostat-coupled modified Robbins device to study biofilms, J. Ind. Microbiol., 15 (1995) 283-289. DOI: 10.1007/bf01569981

[13] H.J. Busscher, H.C. van der Mei, Microbial adhesion in flow displacement systems, Clin. Microbiol. Rev., 19 (2006) 127-141. DOI: 10.1128/CMR.19.1.127-141.2006

[14] S. Perni, E.C. Preedy, P. Prokopovich, Success and failure of colloidal approaches in adhesion of microorganisms to surfaces, Adv. Colloid Interface Sci., 206 (2014) 265-274. DOI: 10.1016/j.cis.2013.11.008

[15] B. Bowen, S. Levine, N. Epstein, Fine particle deposition in laminar flow through parallel-plate and cylindrical channels, J. Colloid Interface Sci., 54 (1976) 375-390. DOI: 10.1016/0021-9797(76)90317-9

[16] J. Camacho-Rodríguez, M.C. Cerón-García, J.M. Fernández-Sevilla, E. Molina-Grima, Genetic algorithm for the medium optimization of the microalga *Nannochloropsis gaditana* cultured to aquaculture, Bioresour. Technol., 177 (2015) 102-109. DOI: 10.1016/j.biortech.2014.11.057

728 [17] A. San Pedro, C.V. González-López, F.G. Acién, E. Molina-Grima, Outdoor pilot
729 production of Nannochloropsis gaditana: Influence of culture parameters and lipid
730 production rates in flat-panel photobioreactors, Algal Res., 18 (2016) 156-165. DOI:
731 10.1016/j.algal.2016.06.011
732 [18] F. García-Camacho, J.J. Gallardo-Rodríguez, A. Sánchez-Mirón, E.H. Belarbi, Y.
733 Chisti, E. Molina-Grima, Photobioreactor scale-up for a shear-sensitive
734 dinoflagellate microalga, Process Biochem., 46 (2011) 936-944. DOI:
735 10.1016/j.procbio.2011.01.005
736 [19] J.J. Gallardo-Rodríguez, M.C. Cerón-García, F. García-Camacho, A. Sánchez-
737 Mirón, E.H. Belarbi, E. Molina-Grima, New culture approaches for yessotoxin
738 production from the dinoflagellate *Protoceratium reticulatum*, Biotechnol. Progr., 23
739 (2007) 339-350. DOI: 10.1021/bp060221u
740 [20] Z. Adamczyk, P. Warszyński, L. Szyk-Warszyńska, P. Weroński, Role of
741 convection in particle deposition at solid surfaces, Colloids Surf. Physicochem. Eng.
742 Aspects, 165 (2000) 157-187. DOI: 10.1016/S0927-7757(99)00416-1
743 [21] E.A. Vogler, Structure and reactivity of water at biomaterial surfaces, Adv. Colloid
744 Interface Sci., 74 (1998) 69-117. DOI: 10.1016/S0001-8686(97)00040-7
745 [22] R.H. Yoon, D.H. Flinn, Y.I. Rabinovich, Hydrophobic interactions between
746 dissimilar surfaces, J. Colloid Interface Sci., 185 (1997) 363-370. DOI:
747 10.1006/jcis.1996.4583
748 [23] J. Moreira, J. Teodósio, F. Silva, M. Simões, L. Melo, F. Mergulhão, Influence of
749 flow rate variation on the development of *Escherichia coli* biofilms, Bioprocess
750 Biosystems Eng., 36 (2013) 1787-1796. DOI: 10.1007/s00449-013-0954-y

751 [24] H. Beyenal, Z. Lewandowski, Internal and external mass transfer in biofilms grown
752 at various flow velocities, Biotechnol. Progr., 18 (2002) 55-61. DOI:
753 10.1021/bp010129s
754 [25] M.C. van Loosdrecht, J. Lyklema, W. Norde, A. Zehnder, Influence of interfaces
755 on microbial activity, Microbiol. Rev., 54 (1990) 75-87.
756 [26] W.G. Characklis, Bioengineering report: fouling biofilm development: a process
757 analysis, Biotechnol. Bioeng., 23 (1981) 1923-1960. DOI: 10.1002/bit.22227
758 [27] S. Dimartino, A.V. Mather, T. Alestra, S. Nawada, M. Haber, Experimental and
759 computational analysis of a novel flow channel to assess the adhesion strength of
760 sessile marine organisms, Interface focus, 5 (2015) 20140059. DOI:
761 10.1098/rsfs.2014.0059
762 [28] J. Azeredo, N.F. Azevedo, R. Briandet, N. Cerca, T. Coenye, A.R. Costa, M.
763 Desvaux, G. Di Bonaventura, M. Hébraud, Z. Jaglic, Critical review on biofilm
764 methods, Crit. Rev. Microbiol., 43 (2017) 313-351. DOI:
765 10.1080/1040841X.2016.1208146
766 [29] R. Sekar, V.P. Venugopalan, K.K. Satpathy, K.V.K. Nair, V.N.R. Rao, Laboratory
767 studies on adhesion of microalgae to hard substrates, Hydrobiologia, 512 (2004) 109-
768 116. DOI: 10.1023/B:HYDR.0000020315.40349.38
769 [30] M. Gross, X. Zhao, V. Mascarenhas, Z. Wen, Effects of the surface physico-
770 chemical properties and the surface textures on the initial colonization and the
771 attached growth in algal biofilm, Biotechnol. Biofuels, 9 (2016) 38. DOI:
772 10.1186/s13068-016-0451-z
773 [31] E.A. Vogler, How Water Wets Biomaterial Surfaces, in: M. Morra (Ed.) Water in
774 biomaterials surface science, John Wiley & Sons, Chichester, 2001, pp. 271-290.

775 [32] A. Ozkan, H. Berberoglu, Physico-chemical surface properties of microalgae,
776 Colloids Surf. B. Biointerfaces, 112 (2013) 287-293. DOI:
777 10.1016/j.colsurfb.2013.08.001

Highlights

1. Microalgal biofouling was monitored with a flow cell attached in closed loop to a PBR
2. PBR biofouling was interpreted using CFD and modelling adhesion dynamics in a flow cell
3. Polyvinyl chloride and stainless steel presented less biofouling than other materials
4. Biofouling may be controlled by limiting the flow of nutrients to the PBR surface